

# Contiguous and Atomically Thin Pt Film with Supra-Bulk Behavior Through Graphene-Imposed Epitaxy

Ji Il Choi, Ali Abdelhafiz, Parker Buntin, Adam Vitale, Alex Robertson, Jamie Warner, Seung Soon Jang,\* and Faisal M. Alamgir\*

The stable atomic configuration and the nature of chemical bonding are investigated in epitaxial Pt films on graphene. Graphene-templated monolayer to few multilayers of Pt, synthesized as contiguous 2D films by room temperature electrochemical methods, is shown both experimentally and computationally to exhibit stable {100} structure in the 1–2 layer range. The fundamental question being investigated is whether surface Pt atoms rendered in these 2D architectures are as stable as those of their counterparts in bulk Pt. Unsurprisingly, a single layer Pt on the graphene (Pt\_1ML/GR) shows much higher Pt dissociation energy of (–7.51 eV) than that of an isolated Pt atom on graphene. However, the dissociation energy from Pt\_1ML/GR shows rather similar energy to that of a Pt(100) surface, –7.77 eV, while in bi-layer Pt on the graphene (Pt\_2ML/GR), this energy decreases to –8.63 eV due to the stronger Pt binding, surpassing its bulk counterpart. At Pt\_2ML/GR, the dissociation energy also slightly surpasses that of bulk Pt(111). Bulk-like stability of atomically thin Pt–graphene is possible through a combination of interplanar Pt–C covalent bonding and inter/intraplanar metallic bonding. This unprecedented stability is also accompanied by a metal-like presence of electronic states at the Fermi level. Such atomically thin metal-graphene architectures can be a new stable platform for synthesizing 2D metallic films with various applications in catalysis, sensing, and electronics.

## 1. Introduction

Among the frontiers of low-dimensional materials systems, one that has remained illusory is a 2D confined, but atomically thin metal film that is contiguous over macroscopic length scales. The case against such structures is obvious. While the highly directional nature of the covalent bonds directs the

planar structure of common 2D materials such as graphene<sup>[1]</sup> and transitional metal dichalcogenides,<sup>[2]</sup> as well as surface/edge templated 2D growth of Au,<sup>[3]</sup> CuCl<sub>2</sub>,<sup>[4]</sup> and ZnO<sup>[5]</sup> nanostructures on/from them, the typically non-directional metallic bonding in metals incentivizes maximizing coordination, i.e., clustering over film growth. The plasticity inherent to the non-directional bonding can lead to 1D<sup>[6]</sup> or 2D<sup>[7]</sup> metal bridge structures when they are limited to within a few tens of atoms. However, it was predicted by Peierls<sup>[8]</sup> more than 80 yr ago that a 2D arrangement of atoms with an extended ordered structure would succumb to thermal fluctuations.

On the other hand, if a metal film growth is directed by a strong covalency with a support, atomically thin metal films may be achievable, but presumably would come at a cost. For example, such a film would sacrifice its metallic nature by introducing an electronic bandgap. From this point of view, a graphene-metal epitaxial architecture is intriguing, since it may be possible for metal valence electrons to hybridize with the  $\pi$  electrons of

graphene, while also retaining significant densities of states at the Fermi level. Our recent discovery of the Pt–graphene epitaxial system<sup>[9–11]</sup> seems to indicate that this hybrid system involves strong bonds (evidenced by an epitaxial strain on the Pt film) but takes on the catalytic properties of Pt itself. Considering metal-graphene epitaxy more broadly in catalyst systems, the graphene interface would lock in a strain condition on the catalyst film while allowing charge transfer through the Dirac cone (if preserved) from a ligand below. We realize that, while the “ligand effect” on a catalyst atom is generally understood to be an electronic effect on that atom from an inorganic/organic species in its atomic vicinity, it would help define the term for our specific case. We define the electronic ligand effect as the change in the local electronic and, thereby, the catalytic properties of a central metal atom brought about by varying its near-neighbor atoms. A definition was used by Robert Burch in his seminal work titled “Importance of Electronic Ligand Effects in Metal Alloy Catalysts<sup>[12]</sup>”, and is a measure of an important vicinity effect. The standard understanding for this ligand effect between (near)surface catalyst metal atoms is derivative

J. I. Choi, A. Abdelhafiz, P. Buntin, A. Vitale, S. S. Jang, F. M. Alamgir  
School of Materials Science and Engineering  
Georgia Institute of Technology  
Atlanta, GA, USA  
E-mail: seungsoon.jang@mse.gatech.edu; faisal.alamgir@mse.gatech.edu

A. Robertson, J. Warner  
Department of Materials  
University of Oxford  
Oxford, UK

The ORCID identification number(s) for the author(s) of this article can be found under <https://doi.org/10.1002/adfm.201902274>.

DOI: 10.1002/adfm.201902274

from the works of Burch and, later, Nørskov and others. For the near surface alloys between Pt and a second metal, Bligaard and Nørskov writes that “the [width of the d-band] changes by the hybridization of the *d*-states of the surface Pt atoms with the second layer atoms. Such an indirect interaction can also be termed a ligand effect.”<sup>[13]”</sup>

Theoretically predicted Sabatier volcano plots for the ligand effect on the canonical reactions such as the oxygen reduction reaction (ORR) could then be directly tuned experimentally. Different metals act catalyst supports induce mechanical strain on atomic-thick Pt adatoms. Strain magnitude and sign (i.e., compressive or tensile) is dictated by the lattice mismatch and crystal structure from underlying metal support.<sup>[14–17]</sup> Pt monolayer supported on Au (111) substrate experienced an increase of Pt–Pt bond distance, indicating presence of tensile strain induced from Au support. On the other hand, Pt monolayer supported on Ir (111) experienced compressive strain as Pt–Pt bond distance was shortened.<sup>[14]</sup> ORR activity of Pt monolayer supported on various metals showed a tight relation to mechanical strain and/of charge transfer from metal support (i.e., ligand effect), where compressive strain and/or electron donation from support to Pt adatoms enhanced ORR activity.<sup>[14,17]</sup>

Metal/graphene architectures will impact not only catalysis, but also electronic, thermoelectric, and optical materials with broad implications and applications in energy and environmental fields. For an architecture where graphene is sitting at the interface between two materials (i.e., support and surface atoms), graphene may not only affect surface metal atoms through epitaxy (i.e., mechanical strain), but can also allow electric field to permeate between the support and surface materials. Kong et al. discussed the effect of single layer graphene to screen the electric field of underlying semiconductor support from surface atoms. Results showed that support-polarity and interaction of graphene with support can surpass graphene’s ability to screen potential.<sup>[18]</sup> We may be able to achieve theoretical limits of interface-dictated properties such as electron/phonon scattering,<sup>[19]</sup> mass transport of most atoms and standard small molecules,<sup>[20]</sup> and near-infinite corrosion resistance, with scale-up potential that leverages roll-to-roll synthesis of continuous monolayer graphene films.<sup>[21]</sup>

Driven by the aforementioned findings, we are presenting a coupled experimental and computational thesis that provides insights about the nature and origin of electronic interactions within monolayer to multilayer (ML) Pt on graphene (Pt<sub>n</sub>ML/GR; *n* = 1, 2, and 3). Particularly, we investigate the nature of the chemical bonds between Pt and graphene that dictates the geometry of the epitaxy, the densities of states at the Fermi level, and the bond energy of surface Pt atoms. On this last issue of the bond energy of surface Pt atoms, the fundamental question we pose is this: is it possible that a combination of metallic and covalent bonding can render the Pt atoms in Pt–graphene more stable than their counterparts in bulk Pt that are supported by metallic bonding? If so, this unprecedented stability would open the door to utilizing epitaxial configurations between metal monolayers and 2D materials as stable platforms where surface chemistry can be tailored for potential applications in catalysis, sensing or electronics.

## 2. Experimental Results

### 2.1. Atomic Structure and Chemical Shifts

Pt and graphene architectures were prepared using chemical vapor deposition and the surface limited redox replacement (SLRR) as per procedures detailed in Supporting Information—Synthesis, while SLRR and its variant, electrochemical atomic layer deposition, have been used in the past to deposit metal on metal by Stickney et al.<sup>[22]</sup>, Brankovic et al.<sup>[23]</sup>, Fayette et al.<sup>[24]</sup>, Alamgir et al. has successfully used it to produce uniform ultrathin platinum layers over various substrates, including bulk metals like gold<sup>[25–27]</sup> and ruthenium,<sup>[28]</sup> oxides such as TiO<sub>2</sub>,<sup>[29]</sup> and 2D materials like graphene.<sup>[9–11]</sup> EXAFS was conducted on Pt<sub>n</sub>ML/GR/Ligand samples at the National Synchrotron Light Source (NSLS Beamline X23A2) and analysis was performed to investigate the Pt atomic near-neighbor structure (Figure 1). Pt foil was used as a reference for the Pt FCC (face-centered cubic) crystal structure in comparison to 1 ML thick Pt grown on graphene and Au (Pt<sub>1</sub>ML/GR/Au). Results showed similar Pt–Pt bond distance for Pt<sub>1</sub>ML/GR/Au and Pt foil for first nearest neighbor, which is possible because of Pt atoms taking advantage of their positional degrees of freedom and relieving stress by buckling out of plane. However, in the radially propagated structure around Pt atoms, we see a compression in the second neighbor distance, corresponding to ≈3% strain in the Pt<sub>1</sub>ML/GR/Au sample in comparison to that of bulk Pt bulk. Moreover, the peak shoulder at lower distance side of the first peak envelope is well aligned with Pt–C bond distance, indicating an intimate Pt–graphene interaction. While the source of EXAFS information is local, the millimeter-sized X-ray probe results in spatially averaged information. Spatially local Pt atomic structure is, therefore, yet to be revealed. In Section 2.2, the detailed nanoscale structure revealed by an aberration-corrected HRTEM in low voltage mode, at 80 KeV which was observed previously to be suitable for characterizing graphene,<sup>[31]</sup> is discussed.

As a test of the through-graphene charge transfer, Pt and Au 4f core level spectra were obtained by XPS (Thermo Scientific K-Alpha with an Al K-α source) from Pt monolayer samples grown directly on single-layer graphene supported on 50 nm Au films on glass slides (see Supporting Information—Synthesis for more information). Figure 1 shows XPS data for Pt that is nominally (\*) 1, 2, and 3 atomic layers thick ML grown by the layer-by-layer SLRR process. The increase in the Pt signal with each additional layer is accompanied by a corresponding decrease in the Au signal, as expected. We further observe the opposing chemical shifts in the Au and Pt 4f<sub>7/2</sub> peak from 2 to 3 nominal multilayers of Pt, indicating that net charge transfer between the substrate and the surface atoms (ligand effect) is dimensionally tunable. Systematic studies of the dimensional tuning of charge transfer to/from Pt monolayer films can be found elsewhere for the graphene-less<sup>[25,27,28]</sup> and the with-graphene cases.<sup>[9,10]</sup> These studies showed that subtle core-level shifts are correlated to the shifts in the observed ORR potentials.

What is clear is the fact that, in these architectures, the graphene imposes the strain condition on the metal monolayer/few-multilayers while also serving as a conduit for charge transfer to/from the support below (the so-called ligand effect).

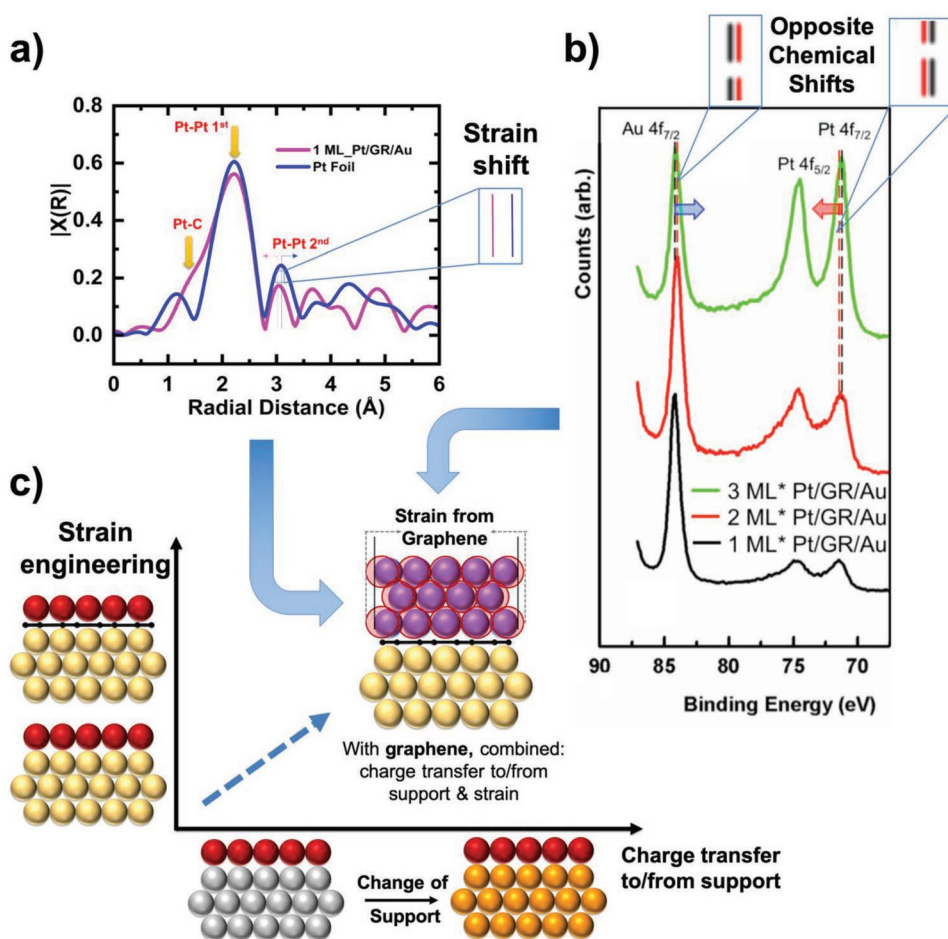


**Figure 1.** a) EXAFS spectra showing compressive strain induced on 1 atomic layer thick Pt adatom supported on graphene/Au substrate (Pt<sub>1ML</sub>/GR/Au) compared to Pt–Pt bond distance of bulk Pt FCC slab. The spectra show bond distance shortening beyond the first nearest neighbor. b) XPS spectra show the chemical shifts due to the charge transfer to/from 1, 2, and 3 nominal (\*) ML of Pt grown on a single layer of Au-supported graphene. The blue and red arrows show opposite shifts ( $\approx \pm 0.3$  eV) in the Au and Pt 4f<sub>7/2</sub> peaks between 2 and 3 ML\* of Pt, indicating that net charge transfer between the support and the surface atoms (ligand effect) is dimensionally tunable. c) schematic representing combined effect of graphene and metal support (i.e., ligand). Charge transfer to/from support is maintained, while mechanical strain is induced by graphene (black line) layer at the interface between surface atoms (purple spheres) and support material (yellow spheres).

Using the graphene as an interrupting interface, therefore, allows one to decouple the strain and ligand effects (Figure 1) imposed on atomically thin metal films.

In a direct observation of the aforementioned ligand effect, ORR activity was probed for electrochemically grown atomic layers Pt<sub>ML</sub> on graphene, supported on different substrates as depicted in Figure 2, where Pt<sub>ML</sub> on graphene foam was used as a control. ORR activity was tracked by following the inflection point of linear sweep voltammetry (LSV) scans. Pt<sub>ML</sub>/GR supported on Au substrate showed lower ORR activity than Pt<sub>ML</sub>/GR support-free samples. Pt<sub>ML</sub>/GR supported on Ni substrate showed the highest ORR performance (with LSV inflection point at the most positive potential). Core@shell structure of Au@Pt with monolayer thick Pt architecture showed lower activity due to electron drainage from Pt adatom, shifting *d*-band center up towards the Fermi level, where reaction intermediates adsorption affinity to catalyst surface is weakened.<sup>[13,32]</sup> Ni@Pt showed remarkable ORR<sup>[33–35]</sup> activity due to shifting *d*-band center down from the

Fermi level (opposite to Au support counterpart).<sup>[10]</sup> The observation reported herein shows striking ORR activity by inducing strain from graphene on metal adatoms, meanwhile, observing ligand effect with through-graphene electron transfer. Thus, graphene proves its flexibility as a support, where the buried ligand underneath influences metal adatoms through the graphene layer but does so de-coupled from the strain condition imposed by the graphene. A de-coupled ligand and strain effect in the Pt/GR system means that, since Pt uses the graphene as its template for epitaxial growth, graphene primarily determines the strain condition on Pt, while the ligand effect is the net charge transfer from the support material (ligand) on the other side of GR. There is, of course, a constant net charge transfer between Pt and graphene, but that constant charge transfer is a part of the coupled strain-ligand effects between Pt and GR.

This exclusive combination of ligand and strain effects opens the door to better control of surface properties and a broader range of applications such as in sensing and electronics.



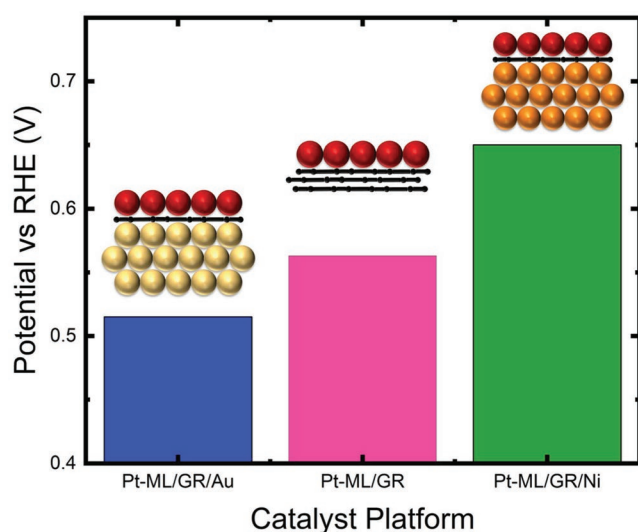


**Figure 2.** ORR inflection point reported for Pt<sub>n</sub>ML/GR platforms supported on different substrates. Blue: Pt<sub>n</sub>ML supported on Au. Pink: Pt<sub>n</sub>ML/GR supported on graphene foam. Green: Pt<sub>n</sub>ML/GR supported on Ni. More positive potential of ORR inflection point indicates smaller overpotential of ORR to occur. These shifts in the ORR overpotential correlate to Pt 4f chemical shifts shown in the Supporting Information.

## 2.2. Microscopy Observations

HRTEM analysis of the Pt ML architecture on single-layer graphene provides insight into both Pt–GR bonding and layer-by-layer epitaxial growth of Pt MLs. Pt monolayers (Pt<sub>n</sub>ML) showed full wetting on graphene surface while avoiding ripening or agglomeration (Figure 3a). Most interestingly, Pt atoms maintain (100) packing structure on graphene, deviating from the most stable crystal orientation of Pt FCC (111). This is due to the nature of the Pt atom registry at the bridge site of graphene's C–C bonds. The Pt–C registry is illustrated by the inset (Figure 3b), which shows the fast Fourier transform (FFT) of the region in Figure 3a. Figure 3c elucidates the atomic stacking showing 1 $\alpha$  (single Pt atom on graphene), 1 $\Phi$  (a monolayer Pt film; Pt<sub>1</sub>ML/GR), and 2 $\Phi$  (the second atomic layer of Pt; Pt<sub>2</sub>ML/GR). The 2 $\Phi$  Pt atoms stack atop the 1 $\Phi$  Pt atoms while retaining the {100} structure. Visible Pt<sub>n</sub>ML/GR atoms are verified to be 1 $\Phi$  or 2 $\Phi$  Pt atoms by multislice image simulations (Figure 3e–h) of the HRTEM image and, from the intensity comparisons in Figure 3h, exclude the possibility of a third layer. The extended film-like nature of the Pt<sub>n</sub>ML/GR is seen in Figure 3d over an approximately 400 nm<sup>2</sup> region. The Pt 2D epitaxy seen here, along with our earlier observation of a Pt–C feature in EXAFS, indicates the existence of a strong chemical interaction (i.e., bonding) between Pt and C.

## 3. Computational Analyses

### 3.1. Simple Cubic Structured Pt Layer on Graphene Template

Forming epitaxial Pt on a graphene template (Pt<sub>n</sub>ML/GR) requires correct description of strong chemical bonding with non-local long-ranged van der Waals (vdW) interactions in the

application of density functional theory (DFT). In the description of structural geometry and electronic properties of low-dimensional materials, difficulty arises as the attractive vdW and strong covalent interactions compete with those of the Coulombic repulsive forces, because the non-bonded weak interactions caused by dynamic electronic correlations in the layered materials have non-trivial effects on the geometry and electronic structures.<sup>[36]</sup> Even though high-level computational methods, such as coupled-cluster singles and doubles with perturbative triples (CCSD(T)) or quantum Monte Carlo, could achieve a full description of the vdW interaction, they are highly demanding for computational resources. Beyond simply using hybrid inter- and intrabonding configuration to include metallic, covalent, and vdW interactions, we employ a newly developed “strongly constrained and appropriately normed” (SCAN)<sup>[37]</sup> meta-generalized-gradient approximation density functional, which is particularly accurate in reproducing inter-layer binding energy, inter- and intralayer lattice constants. Indeed, our initial foray into computing Pt–C bonding at the mono/multilayered-Pt/GR (Pt<sub>n</sub>ML/GR,  $n = 1$  and 2) interface shows significant enhancement of the Pt–C bonding states, predicting the interaction distance to be  $\approx 2$  Å. In addition to the covalent bonds, non-bonded type interactions involved in the Pt and C interaction can be characterized by intermediate and long-ranged vdW non-bonded interaction at the Pt/GR interface. For the description of the long-ranged interactions, non-local correlation from rVV10 vdW density functional<sup>[36]</sup> is employed to calculate interlayer binding energy, and inter- and intralayer lattice constants.

### 3.2. Geometry and Electronic Structures

A chemically stable 2D structure of the Pt<sub>n</sub>ML/GR requires strong binding between the Pt and C atoms in addition to the non-bonded vdW interactions. For single atomic adsorption scenarios (i.e., 1 $\alpha$  in Figure 3), one Pt atom on graphene prefers a chemisorption on twofold bridge site interacting at the distance of 2.10 Å, and needs around  $\approx 2.3$  eV/Pt to dissociate the Pt atom presented in Figure 4, where single point system energies are calculated with respect to the dissociating positions of a Pt atom. The dissociation energy ( $E_D$ ) is defined by the measure of energy depth in the curve, and the reference energy at infinite Pt separation distance is approximated as 0 eV. Lattice dimensions and computational models are provided at Table S1 and Figure S1 of the Supporting Information, respectively. By this definition, a single layer Pt on the graphene (Pt<sub>1</sub>ML/GR) shows much higher dissociation energy of  $-7.51$  eV than that of the single Pt atom on bare graphene surface. The dissociation energy of Pt<sub>1</sub>ML/GR is rather similar to that of Pt(100) surface,  $-7.77$  eV, on which the surface configures Pt atoms in square shape. Bi-layered Pt on the graphene (Pt<sub>2</sub>ML/GR), however, increases the dissociation energy to  $-8.63$  eV which is similar to that of Pt(111),  $-8.56$  eV. Thus, the atomic interactions of the surface Pt atoms on the Pt<sub>1</sub>ML/GR or Pt<sub>2</sub>ML/GR systems are found to provide similar degree of binding to those of Pt(100) and Pt(111), respectively.

In electronic structure, the chemisorption of a Pt atom on bare graphene surface induces the bond elongation between

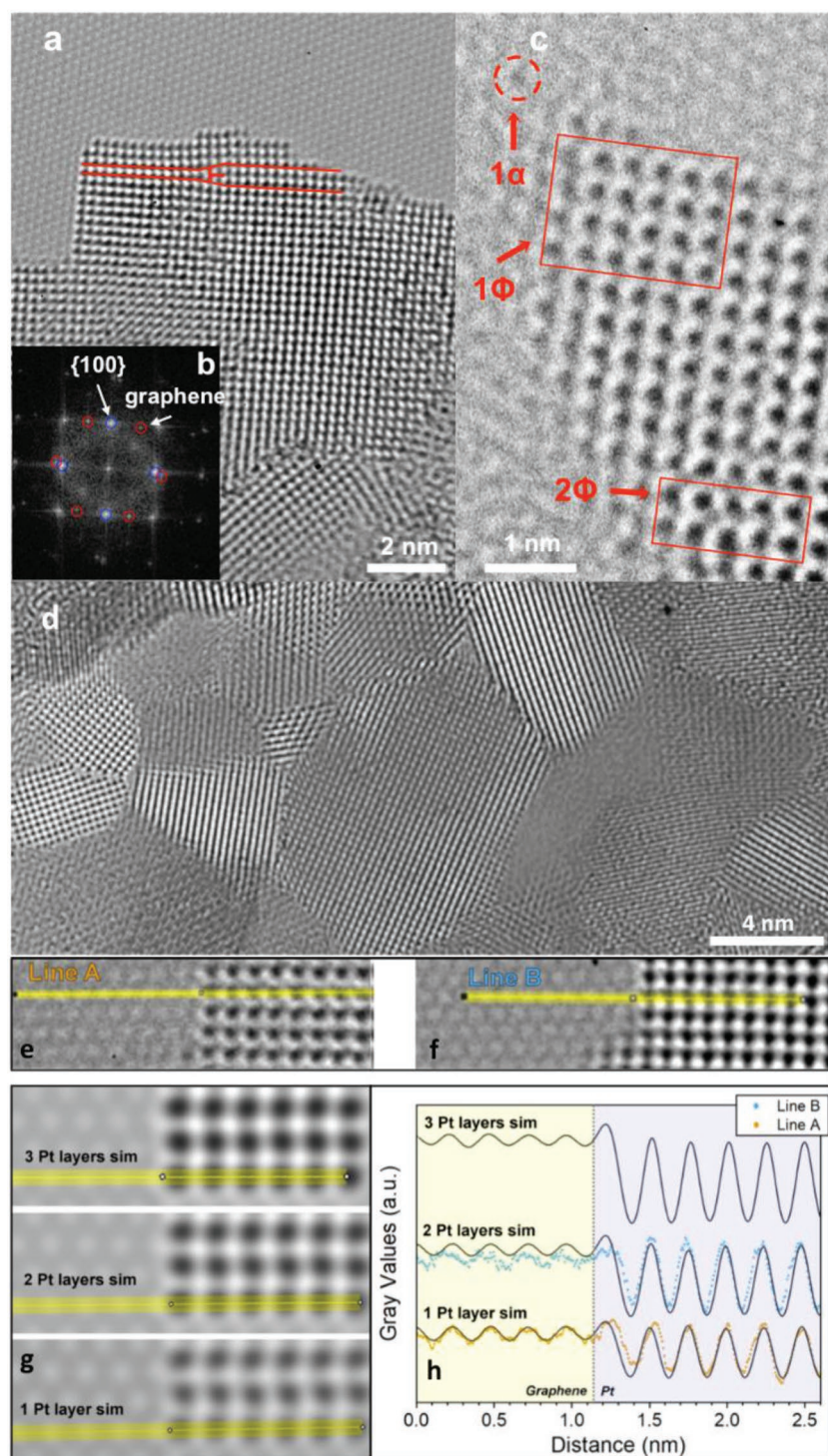


**Figure 3.** TEM image of templated Pt ML on graphene on a) an area of  $\approx 100 \text{ nm}^2$ , Pt ML on graphene, with b) Pt in a  $\{100\}$  epitaxial relation with the underlying graphene as seen by the FFT of the imaged region; c) a closer look at the atomic stacking showing  $1\alpha$  (single Pt atom on graphene),  $1\Phi$  (a monolayer Pt film; Pt\_1ML/GR),  $2\Phi$  (second atomic layer of Pt; Pt\_2ML/GR); d) the contiguous 2D Pt film over  $\approx 400 \text{ nm}^2$  region of Pt showing its grain. Comparison of experimental TEM images with multi-slice image simulations e–h) is shown. Aberration-corrected TEM images e,f) of the edge of Pt layers on a graphene monolayer. Multislice image simulations g) of the edge of three, two, and one Pt layer(s), respectively, on top of a graphene monolayer. h) Intensity line profiles acquired along the indicated lines in e–g). The experimentally acquired profiles are scatter plots, Line A and Line B, and the simulated profiles

carbon atoms bonding with the Pt from 1.42 to 1.52 Å due to the conversion of C(resonance) towards a C( $sp^3$ ) state. Completing one monolayer (1ML) Pt coverage, however, the twofold bonding configuration experiences a transition towards a Pt–C single bond. DFT calculations elaborate structural details and identify the formation of single covalent bond on the bridge position, as seen in Figure 5. Electron density difference ( $\Delta\rho = \rho_{\text{system}} - \rho_{\text{Pt-Layer}} - \rho_{\text{Graphene}}$ ), depicted in Figure 5b, confirms the electron density accumulation at the Pt–C single bonding site. In addition to the Pt–C covalency, developed electron density concatenating Pt atoms implicates the existence of additional bonding characteristics between the Pt atoms. The Pt–C single bond ( $d1$ ) in Figure 5b is found to provide more compact bond length around 1.99 Å, and induces a ripple-shaped deformation to the graphene at atomic scale.

For the Pt–Pt interactions, bound Pt atoms interact with neighbors forming a square shaped grid pattern at more compact distances, 2.39 and 2.54 Å along armchair and zigzag directions, respectively. The shortening of Pt–Pt bonds is evident when compared to that of FCC bulk Pt, 2.77 Å [JCPDS No.04-0802] which is also obtained by the DFT calculation in this study. The expanded graphene dimension as well as the transition of Pt–C bonding configuration implies that the Pt–Pt bonding interaction is a dominant factor in the determination of lattice parameters, which gives  $a = 4.75 \text{ Å}$  along armchair direction and  $b = 5.05 \text{ Å}$  along zigzag direction. The degree of lattice variation is presented by aspect ratio ( $b/a$ ) and is compared to that of pristine graphene in Figure S2b in the Supporting Information.

The electronic structure of the Pt\_nML/GR is developed under a) the structural deformation of graphene, b) monolayered crystalline structure of the Pt, c) the formation of Pt–C covalent bonds, and d) Pt–Pt metallic bond characteristics. Resulting electron density of states (DOS) are projected to Pt( $5d$ ,  $6s$ ) and C( $2p$ ) orbitals in Figure 5c. One noticeable feature is the strong hybridization of Pt( $6s$ ) and C( $2p$ ) orbitals with the Pt( $5d$ ) orbital, and the comparable contribution of each orbital to the DOS at the Fermi level is significant. The band structure shows

are solid lines. The left-hand side of the plots are the line across the graphene lattice, and the right from the Pt crystal. Plots are normalized with respect to the graphene monolayer.



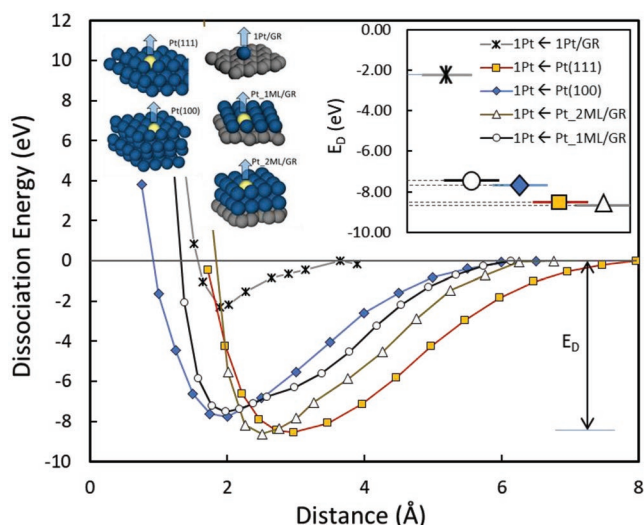


**Figure 4.** Curves for the dissociation energy of a single Pt atom (marked “1Pt ←” in the legend) on the bare graphene, Pt(111), Pt(100), Pt\_1ML/GR, and Pt\_2ML/GR surfaces. The dissociation energy is defined by the depth of each energy plot, where the depth of each configuration is found to be  $-7.51$ ,  $-8.63$ ,  $-7.77$ , and  $-8.56$  eV on the Pt\_1ML/GR, Pt\_2ML/GR, Pt(100), and Pt(111) surfaces, respectively. Single atomic dissociation from the bare graphene surfaces gives  $-2.30$  eV.

projected  $C(2p)$  orbitals well developed near the Fermi level. For practical applications, the covalency between Pt and C implies enhanced efficacy of electron transfer through the normal direction to the surface aside from axial directions.

Energetically favored bi-layer Pt stacking geometries on the graphene (Pt\_2ML/GR) were computed by relaxing the lattice parameters along surface directions and obtained

various geometries with different aspect ratio ( $b/a$ ), as given in Figure S2b in the Supporting Information. When constraining dimensional variations, however, it is found that a simple cubic-like (SC-like) geometry shown in Figure 5a is preserved up to  $a = 4.819$  Å and  $b = 5.155$  Å which correspond to 1.5% and 2.0% expansion of the monolayer dimensions, respectively. As shown in Figure S2a in the Supporting Information, energy minimized structures could exist by rearranging the top Pt layers in more stable energy states with different aspect ratios, keeping the bottom Pt/GR structure intact. The transition to another structure, however, may entail dynamic variation of lattice parameters over the entire system, which requires the Pt-GR architecture to overcome a large structural free energy barrier. Thus, the structures in Figure S2a in the Supporting Information would be determined based on experimental conditions. Of the structures depicted in Figure S2a in the Supporting Information, our computational analysis focuses on the SC-like structure only (Figure 6a) due to observations from experimentally grown Pt\_2ML/GR. Here, it is supposed that the given Pt\_1ML/GR structure plays a role of confining the structural development towards bi-layer Pt stacking, preserving the SC-like structure.

The interaction between Pt and C residing on the Pt\_2ML/GR are found to produce twofold covalent bonds between Pt and C atoms (Pt–2C) of the length  $\approx 2.1$  Å as shown from the single Pt atomic adsorption, regardless of atomic configuration of the second layer, as shown in Figure S1 in the Supporting Information. Figure 6b presents corresponding charge accumulation at the bonding sites for the Pt–2C bonds. It is found that the hybridized energy states among the ( $s$ ,  $p$ ) orbitals are weakened and the  $d$ -band hybridization is not observed. It is thought that the electronic states are more involved in Pt–Pt metallic interactions between Pt layers. For specification, the

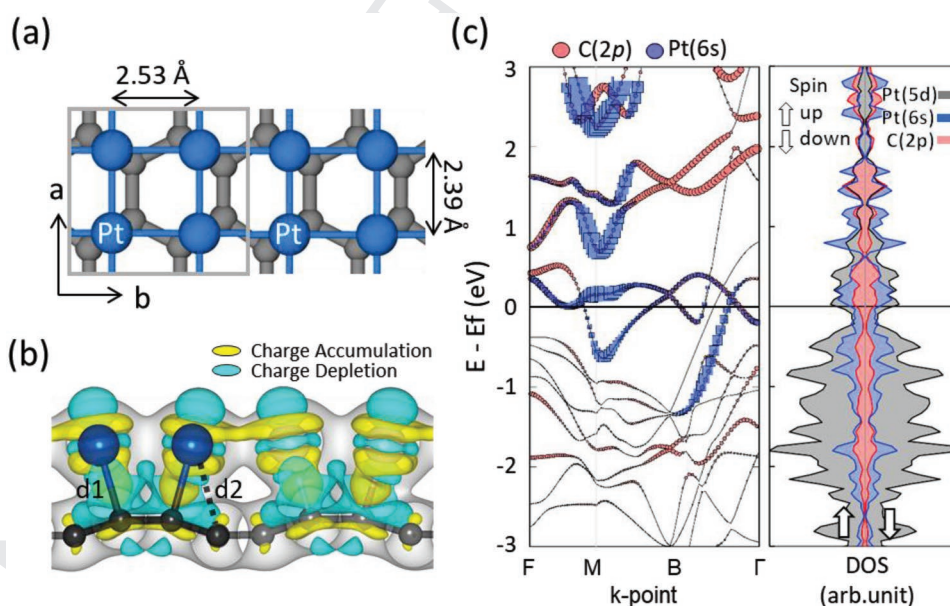


**Figure 5.** Monolayer Pt on graphene (Pt\_1ML/GR) is shown at a) top view and b) side view with charge difference and graphene corrugation induced by the interaction between Pt and graphene. The isosurface is plotted at the level of  $4 \text{ meV Å}^{-3}$ . c) Band structure and spin polarized electronic DOS are projected to the  $C(2p)$ ,  $Pt(5d)$  and  $Pt(6s)$  orbitals. Strongly hybridized orbitals leading to ( $s, p, d$ ) hybridization are shown. The  $Pt(6s)$  bands are partially figured near the Fermi level and conduction bands.

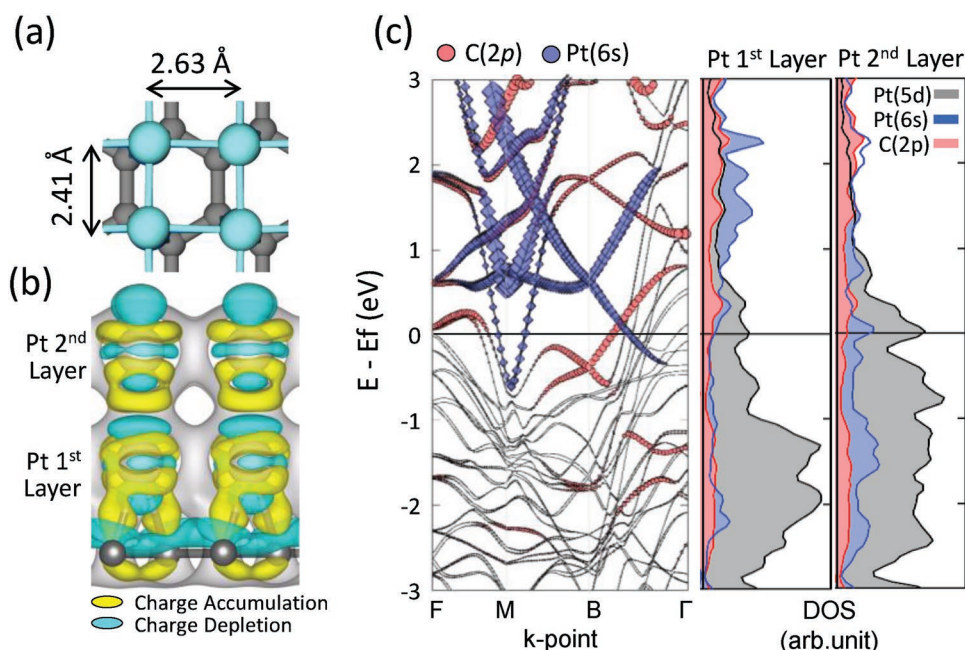


**Figure 6.** Bi-layer Pt on graphene (Pt\_2ML/GR) is shown from a) a top-down view with the dimensional expansion of the bi-layer formation and b) a side view of induced charge density difference by the interactions among the three layers. c) Band structure and projected DOS of C(2p), Pt(5d), and Pt(6s). The first Pt layer interacting with graphene shows similar contributions of the C(2p) and Pt(6s) bands at the Fermi level due to the strong covalent bonds, while the second Pt layer distinguishes the contribution at the Fermi level for each orbital.

electron DOS plot is decomposed into each layer contribution in Figure 6c. Both Pt(6s) and C(2p) orbitals, originating from the interaction between the first layer of Pt and graphene, show equivalent contribution to the Fermi level, while the second layer of Pt shows more metallic behavior at the Fermi level, enhancing the density contributions from Pt(5d) and Pt(6s) orbitals. Comparing the band structure of a bi-layer Pt system with that of monolayer Pt, the C(2p) band near the Fermi level is found to shift down to the valence band while un-hybridized Pt(6s) bands, absent in the monolayer Pt system, are found at the conduction level, as shown in Figure 6c. The *d*-bands<sup>[38,39]</sup> from each Pt layer also show a difference in shape and distribution due to the established bonding type and interaction. The enhanced contribution of the Pt(6s) orbital to the Fermi level distinguishes the electronic structures from the bulk Pt or Pt(111) slab structures given in Figure S3 in the Supporting Information. For the electronic structural change of graphene, both Pt\_1ML/GR and Pt\_2ML/GR systems show induced charge accumulation on the outer surface of graphene, which is expected to facilitate a more active graphene surface in electrochemical reactions.

In summary, we demonstrate contiguous and atomically thin Pt grown epitaxially on graphene. Through a combination of interplanar Pt–C covalent bonding and inter/intraplanar metallic bonding, the Pt–graphene 2D architecture exhibits supra-bulk stability for the surface Pt atoms. This unprecedented atomically thin 2D metal demonstrates a metallic electronic structure via the presence of electronic states at the Fermi level. Such metal-graphene 2D architectures open the door to atomically thin metal films with applications in catalysis, sensing and electronics.

## Supporting Information

Supporting Information is available from the Wiley Online Library or from the author.

## Acknowledgements

J.I.C. and A.A. contributed equally to this work.

## Conflict of Interest

The authors declare no conflict of interest.

## Keywords

band structure, dissociation energy, epitaxy, graphene, strain

Received: March 18, 2019

Revised: August 12, 2019

Published online: 2019

- [1] K. S. Novoselov, A. K. Geim, S. V. Morozov, D. Jiang, S. V. Dubonos, I. V. Grigorieva, A. A. Firsov, *Science* (80-.). **2004**, 306, 666.
- [2] M. K. Jana, C. N. R. Rao, *Philos. Trans. R. Soc., A* . **2016**, 374, 20150318.
- [3] A. W. Robertson, Y. C. Lin, S. Wang, H. Sawada, C. S. Allen, Q. Chen, S. Lee, G. D. Lee, J. Lee, S. Han, E. Yoon, Al. Kirkland, H. Kim, K. Suenaga, J. H. Warner, *ACS Nano* **2016**, 10, 10227.
- [4] S. Wang, H. Li, J. Zhang, S. Guo, W. Xu, J. C. Grossman, J. H. Warner, *ACS Nano* **2017**, 11, 6404.

- [5] H. T. Quang, A. Bachmatiuk, A. Dianat, F. Ortmann, J. Zhao, J. H. Warner, J. Eckert, G. Cuniberti, M. H. Rummeli, *ACS Nano* **2015**, 9, 11408.
- [6] H. Ohnishi, Y. Kondo, K. Takayanagi, *Nature* **1998**, 395, 780.
- [7] J. Zhao, Q. Deng, A. Bachmatiuk, G. Sandeep, A. Popov, J. Eckert, M. H. Rummeli, *Science* (80-), **2014**, 343, 1228.
- [8] R. Peierls, *Ann. I.H.Poincare* **1935**, DOI:12325171.
- [9] A. Abdelhafiz, A. Vitale, P. Buntin, B. deGlee, C. Joiner, A. Robertson, E. M. Vogel, J. Warner, F. M. Alamgir, *Energy Environ. Sci.* **2018**, 11, 1610.
- [10] A. Abdelhafiz, A. Vitale, C. Joiner, E. Vogel, F. M. Alamgir, *ACS Appl. Mater. Interfaces* **2015**, 7, 6180.
- [11] A. Vitale, H. Murad, A. Abdelhafiz, P. Buntin, F. M. Alamgir, *ACS Appl. Mater. Interfaces* **2019**, 11, 1026.
- [12] R. Burch, *Acc. Chem. Res.* **1982**, 15, 24.
- [13] T. Bligaard, J. K. Nørskov, *Electrochim. Acta* **2007**, 52, 5512.
- [14] F. H. B. Lima, J. Zhang, M. H. Shao, K. Sasaki, M. B. Vukmirovic, E. A. Ticianelli, R. R. Adzic, *J. Phys. Chem. C* **2007**, 111, 404.
- [15] J. Song, Z. J. Xiao, Y. C. Jiang, A. A. Abdelhafiz, I. Chang, J. H. Zeng, *Int. J. Hydrogen Energy* **2019**, 44, 11655.
- [16] M. Wu, X. Wu, L. Zhang, A. Abdelhafiz, I. Chang, C. Qu, Y. Jiang, J. Zeng, F. Alamgir, *Electrochim. Acta* **2019**, 306, 167.
- [17] J. Zhang, M. B. Vukmirovic, Y. Xu, M. Mavrikakis, R. R. Adzic, *Angew. Chem., Int. Ed.* **2005**, 44, 2132.
- [18] W. Kong, H. Li, K. Qiao, Y. Kim, K. Lee, Y. Nie, D. Lee, T. Osadchy, R. J. Molnar, D. K. Gaskill, R. L. Myers-Ward, K. M. Daniels, Y. Zhang, S. Sundram, Y. Yu, S. H. Bae, S. Rajan, Y. Shao-Horn, K. Cho, A. Ouagazzaden, J. C. Grossman, J. Kim, *Nat. Mater.* **2018**, 17, 999.
- [19] F. Ruffino, G. Meli, M. G. Grimaldi, *Solid State Commun.* **2016**, 225, 1.
- [20] J. S. Bunch, S. S. Verbridge, J. S. Alden, A. M. van der Zande, J. M. Parpia, H. G. Craighead, P. L. McEuen, *Nano Lett.* **2008**, 8, 2458.
- [21] X. Wu, G. Zhong, L. D'Arsie, H. Sugime, S. Esconjauregui, A. W. Robertson, J. Robertson, *Sci. Rep.* **2016**, 6, 21152.
- [22] C. Thambidurai, Y. G. Kim, J. L. Stickney, *Electrochim. Acta* **2008**, 53, 6157.
- [23] D. Gokcen, S.-E. Bae, S. R. Brankovic, *J. Electrochem. Soc.* **2010**, 157, D582.
- [24] M. Fayette, Y. Liu, D. Bertrand, J. Nutariya, N. Vasiljevic, N. Dimitrov, *Langmuir* **2011**, 27, 5650.
- [25] S. Cheng, R. E. Rettew, M. Sauerbrey, F. M. Alamgir, *ACS Appl. Mater. Interfaces* **2011**, 3, 3948.
- [26] R. E. Rettew, J. W. Guthrie, F. M. Alamgir, *J. Electrochem. Soc.* **2009**, 156, D513.
- [27] R. E. Rettew, S. Cheng, M. Sauerbrey, Th. A. Manz, D. S. Sholl, C. Jaye, D. A. Fischer, F. M. Alamgir, *Top. Catal.* **2013**, 56, 1065.
- [28] J. W. Guthrie, R. E. Rettew, D. Fischer, F. Alamgir, C. Jaye, *ECS Trans.* **2009**, 19, 106.
- [29] R. E. Rettew, N. K. Allam, F. M. Alamgir, *ACS Appl. Mater. Interfaces* **2011**, 3, 147.
- [30] A. Abdelhafiz, A. Vitale, C. Joiner, E. Vogel, F. M. Alamgir, *ACS Appl. Mater. Interfaces* **2015**, 7, 6180.
- [31] H. Kim, A. W. Robertson, S. O. Kim, J. M. Kim, J. H. Warner, *ACS Nano* **2015**, 9, 5947.
- [32] J. Greeley, J. K. Nørskov, *Surf. Sci.* **2005**, 592, 104.
- [33] N. Todoroki, Y. Asakimori, T. Wadayama, *Phys. Chem. Chem. Phys.* **2013**, 15, 17771.
- [34] S. Du, Y. Lu, S. K. Malladi, Q. Xu, R. Steinberger-Wilckens, *J. Mater. Chem. A* **2014**, 2014, 692.
- [35] K. Eid, H. Wang, V. Malgras, Z. A. Allothman, Y. Yamauchi, L. Wang, *Chem.—Asian J.* **2016**, 11, 1388.
- [36] H. Peng, Z. H. Yang, J. P. Perdew, J. Sun, *Phys. Rev. X* **2016**, 6, 041005.
- [37] J. Sun, A. Ruzsinszky, J. Perdew, *Phys. Rev. Lett.* **2015**, 115, 036402.
- [38] B. Hammer, J. K. Nørskov, *Nature* **1995**, 376, 238.
- [39] Y. Fan, K. He, H. Tan, S. Speller, J. H. Warner, *Chem. Mater.* **2014**, 26, 4984.



## Reprint Order Form

**Charges for Reprints in Euro (excl. VAT),** prices are subject to change. Minimum order 50 copies; single issues for authors at a reduced price.

No. of pages	50 copies	100 copies	150 copies	200 copies	300 copies	500 copies
1–4	345,—	395,—	425,—	445,—	548,—	752,—
5–8	490,—	573,—	608,—	636,—	784,—	1077,—
9–12	640,—	739,—	786,—	824,—	1016,—	1396,—
13–16	780,—	900,—	958,—	1004,—	1237,—	1701,—
17–20	930,—	1070,—	1138,—	1196,—	1489,—	2022,—
every additional 4 pages	147,—	169,—	175,—	188,—	231,—	315,—

Manuscript No.: \_\_\_\_\_  
Customer No.: (if available) \_\_\_\_\_  
Purchase Order No.: \_\_\_\_\_  
Author: \_\_\_\_\_

**Information regarding VAT:** The charges for publication of *cover pictures / reprints / issues / poster / Video abstracts /* are considered to be “supply of services” and therefore subject to German VAT. However, if you are an institutional customer outside Germany, the tax can be waived if you provide us with the valid VAT number of your company. Non-EU customers may have a VAT number starting with “EU” instead of their country code, if they are registered with the EU tax authorities. If you do not have a valid EU VAT number and you are a taxable person doing business in a non-EU country, please provide a certification from your local tax authorities confirming that you are a taxable person under local tax law. Please note that the certification must confirm that you are a taxable person and are conducting an economic activity in your country. **Note:** certifications confirming that you are a tax-exempt legal body (non-profit organization, public body, school, political party, etc.) in your country do not exempt you from paying German VAT.

Please send me send bill me for

☐ no. of reprints

☐ no. of issue  
(1 copy: 28 Euro)

☐ high-resolution PDF file (330 Euro excl. VAT)  
E-mail address: \_\_\_\_\_

❖ Special Offer:

If you order 200 or more reprints you will get  
a PDF file for half price.

*Please note: It is not permitted to present the PDF file on  
the internet or on company homepages.*

**Cover Posters** (prices excl. VAT)

Posters of published covers are available in two sizes:

☐ DIN A2 42 x 60 cm / 17 x 24in (one copy: 39 Euro)

☐ DIN A1 60 x 84 cm / 24 x 33in (one copy: 49 Euro)

**Postage for shipping** (prices excl. VAT)

overseas +25 Euro  
within Europe +15 Euro

VAT number: \_\_\_\_\_

Mail reprints / copies of the issue to:

\_\_\_\_\_  
\_\_\_\_\_  
\_\_\_\_\_  
\_\_\_\_\_

Send bill to:

\_\_\_\_\_  
\_\_\_\_\_  
\_\_\_\_\_  
\_\_\_\_\_

☐ I will pay by bank transfer

☐ I will pay by credit card

**VISA, Mastercard and AMERICAN EXPRESS**

For your security please use this link (Credit Card  
Token Generator) to create a secure code Credit  
Card Token and include this number in the form  
instead of the credit card data. Click here:

[https://www.wiley-vch.de/editorial\\_production/index.php](https://www.wiley-vch.de/editorial_production/index.php)

**CREDIT CARD TOKEN NUMBER**

						V													
--	--	--	--	--	--	---	--	--	--	--	--	--	--	--	--	--	--	--	--

Date, Signature \_\_\_\_\_